Available online at www.sciencedirect.com
SCIENCE DIRECT®
Advances in Water Resources 27 (2004) 57–69
Advances in Water Resources
www.elsevier.com/locate/advwatres

Reduced models for linear groundwater flow models using empirical orthogonal functions

P.T.M. Vermeulen [a,*], A.W. Heemink [a], C.B.M. Te Stroet [b]

[a] Faculty of Information Technology and Systems, Delft University of Technology, P.O. Box 5031, 2600 GA Delft, The Netherlands
[b] Netherlands Institute of Applied Geoscience TNO, National Geological Survey, P.O. Box 6012, 2600 JA Delft, The Netherlands

Received 11 September 2002; received in revised form 18 August 2003; accepted 1 September 2003

Abstract

In this paper we describe two reduced models that describe the hydraulic head **h** within three-dimensional groundwater flow models. We defined a reduced model structure as a linear combination of a set of spatial patterns **P** with time-varying coefficients **r**. The patterns were obtained by a data-driven indentification technique (Empirical Orthogonal Functions, EOFs), and they span a subspace of model results that captures most of the relevant information of the original model. Due to those patterns, we constructed two different formulations for $d\mathbf{r}/dt$, by applying different projections: (1) a State-Space Projection (SSP) that projects a state-space formulation for groundwater flow; and (2) a Galerkin Projection (GP) that substitutes **h** within the PDE for groundwater flow by the reduced model structure $\mathbf{P}^T\mathbf{r}$, and projects the outcome onto the patterns. The SSP and GP have been both applied to a realistic case study with a negligible loss of model accuracy (Relative Mean Absolute Error < 0.5%). The dimension of **r** (16) was significantly reduced compared to the dimension of **h** (32,949) and hence we achieved a maximal reduction in computational time for the SSP ≈ 1/625 and for the GP ≈ 1/70 of the original time. Both reduced models have a promising prospect as their time reduction increases whenever the number of grid cells increases and the parameterization of the original model grows in complexity.

Keywords: Groundwater; MODFLOW; Empirical orthogonal functions; Reduced model; Galerkin projection; State-space projection

1. Introduction

Currently, the availability and accuracy of the digital subsurface data sets allow the use of numerical groundwater models with a large number of grid cells (often >1 million). Such large models have long computational times for transient problems. Apparently, the advantage of digital data becomes a disadvantage when we need to evaluate the model for many different cases, for example to optimize scenarios. Especially in such a case, our objective should not be to formulate an overly accurate mathematical model, but to formulate a model that is useful for the intended study. From this perspective, Newman [11] stated: "We may wish to sacrifice some of the correctness of the model in order to make the equations easier to solve, or to allow a faster computation". Such a reduced model structure may consist of a set of spatial *patterns* with *time-dependent coefficients*. As the number of coefficients are less, compared to the number of original equations, a significant reduction in computational time can be achieved.

Patterns. There are several methods to define patterns, such as analytical and data-driven techniques. An advantage of analytical patterns (such as Fourier functions, wavelets or polynomials) is that they are defined a priori, but they are disadvantageous with respect to the number of patterns required [2]. The number of patterns can be minimized whenever we use a data-driven technique. Of course, this can be disadvantageous too because the data should be generated with the original model. In the different fields of science, the data-driven pattern identification technique is also called Empirical Orthogonal Functions (EOFs) [17], Coherent Structures (CS) [16], Principal Component Analysis (PCA), Common Factor Analysis (CFA) [15] or Proper Orthogonal Decomposition (POD) [2,4,7]. Hooimeijer [8] described the different pattern identification techniques (data driven and analytical) extensively. He selected the EOF technique (or its data-driven equivalent) as being the

* Corresponding author.
E-mail addresses: p.vermeulen@nitg.tno.nl (P.T.M. Vermeulen), a.w.heemink@its.tudelft.nl (A.W. Heemink), c.testroet@nitg.tno.nl (C.B.M. Te Stroet).

0309-1708/$ - see front matter © 2003 Elsevier Ltd. All rights reserved.
doi:10.1016/j.advwatres.2003.09.008

most suitable one to create a reduced model. In this paper we describe and implement the EOF technique for numerical groundwater flow.

Time-dependent coefficients. The second part of the reduced model structure consists of time-dependent coefficient that can be obtained by *projecting* an existing system equation upon a set of patterns. This projection technique is not new and has been mathematically described by Newman [11]. It has been applied in a wide range of scientific fields, such as turbulence and image processing by Sirovich [16], rapid thermal chemical vapor deposition by Adomaitis [1] and in fluid dynamics for a lid-driven cavity with a rotating rod by Hoffman Jørgensen and Sørensen [7] and Cazemier et al. [2]. They substituted a reduced model structure within their partial differential equation (PDE) and projected the outcome onto the patterns. We call this a *Galerkin Projection* or Karhunen–Loève Expansion. In this paper we apply a Galerkin projection for the hydraulic head within a PDE for groundwater flow. We compare the time-dependent coefficients obtained from this technique with those elaborated earlier by Vermeulen et al. [18–20]. They applied a *State-Space Projection* for a state-space formulation for groundwater flow.

The reduced model construction methodology is given in Fig. 1.

It starts with a collection of scenarios that needs to be computed, for example different pumping strategies. With that in mind, we compute several model evaluations (called *snapshots* [16]) with the original model MODFLOW [10], from which we extract patterns (EOFs). We use those patterns, together with the mathematical formulation and system properties of the original model, to create a reduced model. The formulation of the reduced model depends on the chosen projection strategy: (1) a State-Space Projection (SSP) whereby we project a state-space formulation of groundwater flow; or (2) a Galerkin Projection (GP) whereby we project the PDE for groundwater flow. In practice, verification of the reduced model can lead to a refinement of the snapshots and/or to the selection of more or different patterns. Finally, the reduced model is capable of simulating the collection of scenarios with a significant time reduction.

2. Reduced model

In this section we describe the mathematical formulation for the reduced model structure and two different reduced models that are both capable to represent the hydraulic head as a collection of time-dependent coefficients. The reduced models are both based upon the finite-difference formulation of groundwater flow as applied in MODFLOW [10].

2.1. Formulation of groundwater flow

To describe groundwater flow in three dimensions with a uniform density and viscosity, we use the partial differential equation based upon Darcy's law and the equation of continuity:

$$\frac{\partial}{\partial x}\left(K^x\frac{\partial h}{\partial x}\right)+\frac{\partial}{\partial y}\left(K^y\frac{\partial h}{\partial y}\right)+\frac{\partial}{\partial z}\left(K^z\frac{\partial h}{\partial z}\right)-q^s=S^s\frac{\partial h}{\partial t}, \tag{1}$$

where h represents the hydraulic head (L); K^x, K^y, K^z are the hydraulic conductivities in x, y, z direction (LT^{-1}); S^s is the specific storage, or volume of water released from storage in a unit of aquifer per unit decline in head (L^{-1}); t is time (T); q^s is a fluid source/sink term, or the volumetric rate at which water is added to or removed from the system per unit volume of aquifer (T^{-1}) described by:

$$q^s=w^s+C^s(h-h_{riv}), \tag{2}$$

where w^s is the constant volumetric discharge or recharge from the system per unit volume of aquifer (T^{-1}); C^s represents the conductance per unit volume of aquifer between a surface water element and the hydraulic head ($L^{-1}T^{-1}$); and h_{riv} is the corresponding water level in the surface water element (L).

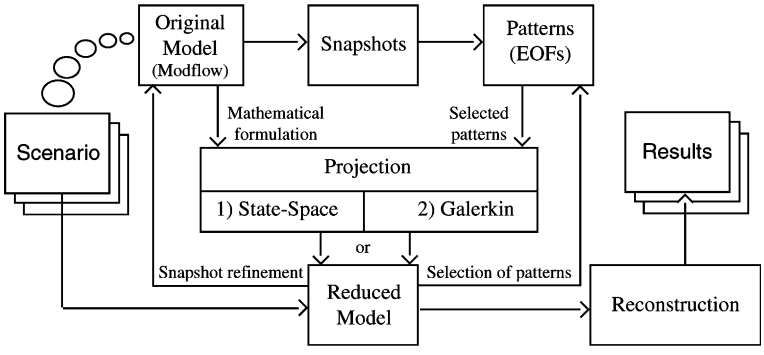

Fig. 1. Methodology for constructing a reduced model.

2.2. Formulation of a reduced model structure

A reduced model structure is based upon the assumption that the hydraulic head can be expressed in terms of a set of spatially distributed patterns with time-varying coefficients. Hence, this approximated hydraulic head $\hat{h}$ can be described by:

$$\hat{h}(\underline{x},t) = h_*(\underline{x}) + \sum_{n=1}^{n_p} p_n(\underline{x}) r_n(t) \tag{3}$$

where $\underline{x}$ is the location in Euclidean space; h_* is the reference hydraulic head (L); p_n is the nth pattern value out of n_p (–); and r_n is the nth time-dependent coefficient (L). For this type of model structure, the spatial distribution of the patterns are captured once, and hence we need to compute only n_p coefficients r over time t.

In several cases, the external sources q^s (wells, rivers, e.g.) and boundary conditions (constant hydraulic heads) can be grouped into:

(1) *Fixed impulses* that remain constant in time. These impulses are not described by patterns but are represented by a reference head h_*. They represent a steady-state solution of the original model, with those impulses that *will not* be varied within the reduced model (variables notated with a superscript f);
(2) *Pattern impulses* that are time varying. These impulses are represented by the patterns p and *can/will* be simulated with the reduced model (variables notated with a superscript p).

A relationship exists between the patterns and the model parameterization described by K^x, K^y, K^z, S^s and C^s. Whenever one of those parameters are changed, we need to identify a new reference head and a set of patterns. The patterns remain valid whenever the variables h_{riv} and w^s (actually the driving forces) are varied, *but* the patterns need to be reindentified whenever the positions for h_{riv} and/or w^s are changed.

2.3. Pattern identification (EOFs)

To compute EOFs, we create an empirical data set in which n_e solutions of the original steady-state or transient MODFLOW model are arranged in vectors, called *snapshots*. They describe a specific behaviour of the hydraulic head that need to be simulated in the future by the reduced model (e.g. the draw-down of the extraction well). Each row within a snapshot represents the hydraulic head for a specific *active* grid cell in the model (n_m). Grid cells that are in-active and/or have a constant hydraulic head are excluded; within MODFLOW these grid cells have an IBOUND value of $\leqslant 0$. The chosen snapshots will influence the accuracy of the reduced model [12] and should be chosen with care. From a numerical point of view, snapshots should be (almost) uncorrelated, because it leads to a better posed eigenproblem [2]. On the other hand, it is a challenge to minimize n_e so less computations have to be performed with the original model. In Section 3.2 a strategy is described to collect those snapshots that is earlier described by Vermeulen et al. [19,20].

We store the ensemble of snapshots within a matrix $\mathbf{H} = [\mathbf{h}_1, \mathbf{h}_2, \ldots, \mathbf{h}_{n_e}]$. We substract $\mathbf{h}_*$ from each snapshot vector as the resulting patterns are superpositioned upon the reference head (3). Thereafter we weigth/scale the result upon its vector length ($\|\mathbf{h}_n - \bar{\mathbf{h}}\|$) as snapshot vectors with large values for h will overrule those with tiny values [11]. Within an EOF analyses the regularity that exists within a snapshot is more important than its amplitude. So, for each vector $\mathbf{h}_n$ we create a new vector $\mathbf{d}_n$ such that:

$$\mathbf{d}_n = \frac{1}{\|\mathbf{h}_n - \mathbf{h}_*\|}(\mathbf{h}_n - \mathbf{h}_*) \tag{4}$$

We collect the centered and weighted vectors as columns in $\mathbf{D} = [\mathbf{d}_1, \mathbf{d}_2, \ldots, \mathbf{d}_{n_e}]$ and mathematically, the EOFs are the eigenvectors of the covariance matrix of $\mathbf{D}$. The eigenvalues provide a measure of the relative "energy" associated with a corresponding eigenvector (EOF/pattern). This measure can also be interpreted as the relative amount of time that the hydraulic head spends along the corresponding pattern. To avoid the computational expense of solving the eigenvalue problem for a very high-dimensional covariance matrix $\mathbf{C}_d = \mathbf{D}\mathbf{D}^T$, we define a matrix $\mathbf{C}_s = \mathbf{D}^T\mathbf{D}$ as a *minor* product of $\mathbf{D}$ [9] and solve a "reduced" eigenvalue problem:

$$\mathbf{C}_s\mathbf{g}_n = \mathbf{g}_n\lambda_n, \quad n \in \{1, \ldots, n_e\}. \tag{5}$$

We transform the eigenvectors $\mathbf{G}$ of $\mathbf{C}_s$ with dimension n_e into eigenvectors $\mathbf{V}$ with dimension n_m by applying [5]:

$$\mathbf{V} = \mathbf{D}\mathbf{G}\mathbf{\Lambda}^{-\frac{1}{2}}, \tag{6}$$

where $\mathbf{\Lambda}^{-\frac{1}{2}}$ is the square root of the inverse of a matrix with eigenvalues λ on the main diagonal. The eigenvectors and eigenvalues are equal to those that would have been obtained by an eigenvalue decomposition of $\mathbf{C}_d$. Eventually, each pattern $\mathbf{p}_n$ is a normalized eigenvector, so $\mathbf{p}_n = \|\mathbf{v}_n\|^{-1}\mathbf{v}$. Its importance is given by:

$$\varphi_n = \frac{\lambda_n}{\sum_{m=1}^{n_e}\lambda_m} \cdot 100\%, \quad n \in \{1, \ldots, n_e\}. \tag{7}$$

From a mathematical point of view, the reduced model structure should be able to reproduce at least that amount of model variance as explained totally by a selected set of n_p patterns. We call this the expected variance, defined by: $\varphi^e = \sum_{n=1}^{n_p}\varphi_n$. From experiences it appeared that it should be at least 99% to obtain reliable time-dependent coefficients. So, we collect n_p patterns such that $\varphi_1 > \varphi_2 > \cdots > \varphi_{n_p} \geqslant 99\%$ and store their corresponding patterns as columns within

$\mathbf{P} = [\mathbf{p}_1, \mathbf{p}_2, \ldots, \mathbf{p}_{n_p}]$. The $[n_m \times n_p]$ dimensional matrix $\mathbf{P}$ is *orthonormal*, which means that all patterns are perpendicular to each other ($\mathbf{P}^{\mathrm{T}}\mathbf{P} = \mathbf{I}$). The projection matrix $\mathbf{P}$ can be seen as a system of axes that describe/span the original model most optimal.

2.4. Dynamic reduced model

To compute the time-dependent coefficients r existing in the reduced model structure (3), we define an ordinary differential equation (ODE) that describes $\mathrm{d}r/\mathrm{d}t$:

$$fr - \underline{q} = \frac{\mathrm{d}r}{\mathrm{d}t}, \tag{8}$$

where f is a linear function that determines how r evolutes with t, and $\underline{q}$ is a forcing term that operates in the reduced model, comparable to q^{s} (1). In this paper we discuss two strategies to compute $\mathrm{d}r/\mathrm{d}t$:

(1) *State-space projection SSP:* (Section 2.4.1) we project a discretized state-space formulation of groundwater flow. Although the projection consumes more time to complete, it has an advantage in a numerical point of view (Section 2.5), and it leads to a reduced model that computes faster than the one created by a GP. This projection has been already succesfully applied to groundwater flow [18–20];
(2) *Galerkin projection GP:* (Section 2.4.2) we substitute h within the PDE for groundwater flow (1) by the reduced model structure (3) and project the outcome onto the patterns. The GP can be thought of as the more elementary method of the two, since it results in an ODE for $\mathrm{d}r/\mathrm{d}t$ prior to the projection. This type of projection has been successfully applied within different sciences [1,2,4,7,12].

2.4.1. State-space projection (SSP)

One way to solve the continuous formulation for groundwater flow is to discretize the PDE in space and time using finite-differences. To express the finite-difference approximation for the space and time derivative of the hydraulic head, we discretize the PDE (1) for each grid cell in a mesh wherein each node is indexed by a row (i), column (j) and layer (k) number:

$$\begin{aligned}
&\Big(- C^{\mathrm{r}}_{(i,j-\frac{1}{2},k)} - C^{\mathrm{r}}_{(i,j+\frac{1}{2},k)} - C^{\mathrm{c}}_{(i-\frac{1}{2},j,k)} - C^{\mathrm{c}}_{(i+\frac{1}{2},j,k)} - C^{\mathrm{v}}_{(i,j,k-\frac{1}{2})} \\
&\quad - C^{\mathrm{v}}_{(i,j,k+\frac{1}{2})} - \frac{1}{\Delta t^m} S_{(i,j,k)} - C_{(i,j,k)} \Big) h^m_{(i,j,k)} + C^{\mathrm{r}}_{(i,j-\frac{1}{2},k)} h^m_{(i,j-1,k)} \\
&\quad + C^{\mathrm{r}}_{(i,j+\frac{1}{2},k)} h^m_{(i,j+1,k)} + C^{\mathrm{c}}_{(i-\frac{1}{2},j,k)} h^m_{(i-1,j,k)} + C^{\mathrm{c}}_{(i+\frac{1}{2},j,k)} h^m_{(i+1,j,k)} \\
&\quad + C^{\mathrm{v}}_{(i,j,k-\frac{1}{2})} h^m_{(i,j,k-1)} + C^{\mathrm{v}}_{(i,j,k+\frac{1}{2})} h^m_{(i,j,k+1)} \\
&= W_{(i,j,k)} - \frac{1}{\Delta t^m} S_{(i,j,k)} h^{m-1}_{(i,j,k)} - C_{(i,j,k)} h_{\mathrm{riv}(i,j,k)},
\end{aligned} \tag{9}$$

wherein

$$C^{\mathrm{c}}_{(i\pm1,j,k)} = \frac{2\,\Delta x_{(j)}\,\Delta z^2_{(k)} K^y_{(i,j,k)} K^y_{(i\pm1,j,k)}}{K^y_{(i,j,k)}\,\Delta z_{(k)}\,\Delta y_{(i\pm1)} + K^y_{(i\pm1,j,k)}\,\Delta z_{(k)}\,\Delta y_{(i)}}, \tag{10}$$

$$C^{\mathrm{r}}_{(i,j\pm1,k)} = \frac{2\,\Delta y_{(i)}\,\Delta z^2_{(k)} K^x_{(i,j,k)} K^x_{(i,j\pm1,k)}}{K^x_{(i,j,k)}\,\Delta z_{(k)}\,\Delta x_{(j\pm1)} + K^x_{(i,j\pm1,k)}\,\Delta z_{(k)}\,\Delta x_{(j)}}, \tag{11}$$

$$C^{\mathrm{v}}_{(i,j,k\pm1)} = \left(\Delta x_{(j)}\,\Delta y_{(i)}\right) \Bigg/ \left(\frac{\frac{1}{2}\Delta z_{(k\pm1)}}{K^{\mathrm{v}}_{(i,j,k\pm1)}} + \frac{\Delta z^{\mathrm{s}}_{(k\pm1)}}{K^{\mathrm{s}}_{(i,j,k\pm1)}} + \frac{\frac{1}{2}\Delta z_{(k)}}{K^{\mathrm{v}}_{(i,j,k)}} \right). \tag{12}$$

Herein C^{r}, C^{c}, C^{v} are the confined harmonic mean hydraulic conductances ($\mathrm{L}^2\mathrm{T}^{-1}$) between nodes along the rows, columns and layers, respectively; Δx, Δy, Δz are the dimensions of a grid cell along the columns, rows and layers, respectively (L); K^{v} is the vertical hydraulic conductivity of an aquifer; K^{s} is the vertical hydraulic conductivity of a semiconfining unit (clay e.g.) between two aquifers; W is the source/sink term ($\mathrm{L}^3\mathrm{T}^{-1}$); the storage coefficient S ($\mathrm{L}^2\mathrm{T}^{-1}$) and the streambed conductance of a surface water element C ($\mathrm{L}^2\mathrm{T}^{-1}$) are defined as:

$$S_{(i,j,k)} = S^{\mathrm{s}}_{(i,j,k)}\,\Delta x_{(j)}\,\Delta y_{(i)}\,\Delta z_{(k)}, \tag{13}$$

$$C_{(i,j,k)} = C^{\mathrm{s}}_{(i,j,k)} O_{(i,j,k)}, \tag{14}$$

where O is the wetted area of the streambed times the total length of the river element in the corresponding grid cell (L^3). Because (9) involves up to seven unknown values of hydraulic head, the equations for the entire model grid must be solved simultaneously at each time step m. This entire set of equations can be summarized in matrix form as:

$$\mathbf{A}\mathbf{h}^m = -\frac{1}{\Delta t}\mathbf{S}\mathbf{h}^{m-1} + \mathbf{w}^m - \mathbf{C}\mathbf{h}^m_{\mathrm{riv}}, \tag{15}$$

and is often solved by using an iterative procedure. It is also possible to rewrite (15) according to:

$$\mathbf{h}^m = -\frac{1}{\Delta t}\mathbf{A}^{-1}\mathbf{S}\mathbf{h}^{m-1} + \mathbf{A}^{-1}(\mathbf{w} - \mathbf{C}\mathbf{h}_{\mathrm{riv}})^m. \tag{16}$$

The advantage of (16) is that we find the solution vector $\mathbf{h}^m$ by matrix multiplication only. Though it is highly unusual that someone would ever simulate such formulation as it is computationally very demanding. Its dreary characteristic ($\mathbf{A}^{-1}$) can be overcome whenever we multiply (*project*) the entire equation with the selected set of patterns $\mathbf{P}$. In this approach $\mathbf{P}^{\mathrm{T}}$ acts as a *reductor* that reduces an n_m dimensional vector into an n_p dimensional vector; $\mathbf{P}$ itself acts as a *reconstructor* that performs the reverse operation. To reduce a matrix we first multiply it with $\mathbf{P}^{\mathrm{T}}$ and thereafter with $\mathbf{P}$. Eq. (16) looks then like:

$$\underbrace{\mathbf{P}^{\mathrm{T}}\mathbf{h}^{m}}_{\mathbf{r}^{m}} = -\frac{1}{\Delta t}\mathbf{P}^{\mathrm{T}}\mathbf{A}^{-1}\mathbf{S}\mathbf{P}\underbrace{\mathbf{P}^{\mathrm{T}}\mathbf{h}^{m-1}}_{\mathbf{r}^{m-1}} + \mathbf{P}^{\mathrm{T}}\mathbf{A}^{-1}\underbrace{\left(\mathbf{w}^{\mathrm{p}} - \mathbf{C}^{\mathrm{p}}\left(\mathbf{h}^{\mathrm{p}}_{\mathrm{riv}} - \mathbf{h}_{*}\right)\right)}_{\mathbf{b}^{\mathrm{p}}}{}^{m}, \tag{17}$$

where the superscript p indicates that they represent *pattern impulses* (Section 2.2). Unfortunately, we cannot solve (17) as long as we need to compute $\mathbf{A}^{-1}$, therefore we rewrite it as:

$$\mathbf{r}^{m} = -\frac{1}{\Delta t}\left(\mathbf{A}^{-\mathrm{T}}\mathbf{P}\right)^{\mathrm{T}}\mathbf{S}\mathbf{P}\mathbf{r}^{m-1} + \left(\mathbf{A}^{-\mathrm{T}}\mathbf{P}\right)^{\mathrm{T}}(\mathbf{b}^{\mathrm{p}})^{m} \tag{18}$$

and, instead of computing $\mathbf{A}^{-\mathrm{T}}$ (the transpose of the inverse) completely, we define a matrix $\mathbf{M}$ with dimension $[n_m \times n_p]$ as:

$$\mathbf{M} = \mathbf{A}^{-\mathrm{T}}\mathbf{P}, \tag{19}$$

for which we solve each vector $\mathbf{m}_n$ in $\mathbf{M}$, so:

$$\mathbf{A}^{\mathrm{T}}\mathbf{m}_n = \mathbf{p}_n, \quad n \in \{1, \ldots, n_p\}. \tag{20}$$

It should be noticed that it is not difficult to implement (20) within MODFOW as $\mathbf{A}^{\mathrm{T}} = \mathbf{A}$ and hence we need to exchange the right-hand side within (15) by $\mathbf{p}_n$. We can now rewrite (18) as:

$$\boxed{\mathbf{r}^{m} = \underbrace{-\frac{1}{\Delta t}\mathbf{M}^{\mathrm{T}}\mathbf{S}\mathbf{P}}_{\mathbf{N}}\mathbf{r}^{m-1} + \left(\mathbf{M}^{\mathrm{T}}\mathbf{b}^{\mathrm{p}}\right)^{m}.} \tag{21}$$

We call this a reduced model that simulates a finite-difference approximation of $\mathrm{d}\mathbf{r}/\mathrm{d}t$ (8) based upon a state-space formulation of groundwater flow [18–20]. The computation of $\mathbf{r}^{m}$ consists finally of a time-dependent projection of $\mathbf{b}^{\mathrm{p}}$ with $\mathbf{M}^{\mathrm{T}}[n_p \times n_m]$, and a multiplication of the previous coefficient $\mathbf{r}^{m-1}$ with $\mathbf{N}[n_p \times n_p]$.

2.4.2. Galerkin projection (GP)

The Galerkin Projection or Karhunen–Loève Expansion substitutes the hydraulic head h within the original PDE ((1) and (2)) by the reduced model structure (3). This results in the formulation:

$$\frac{\partial}{\partial x}\left(K^{x}\frac{\partial\left(h_{*} + \sum_{n=1}^{n_p} p_n r_n\right)}{\partial x}\right) + \frac{\partial}{\partial y}\left(K^{y}\frac{\partial\left(h_{*} + \sum_{n=1}^{n_p} p_n r_n\right)}{\partial y}\right) + \frac{\partial}{\partial z}\left(K^{z}\frac{\partial\left(h_{*} + \sum_{n=1}^{n_p} p_n r_n\right)}{\partial z}\right) - w^{\mathrm{s}} - C^{\mathrm{s}}\left(\left(h_{*} + \sum_{n=1}^{n_p} p_n r_n\right) - h_{\mathrm{riv}}\right) = S^{\mathrm{s}}\frac{\partial\left(h_{*} + \sum_{n=1}^{n_p} p_n r_n\right)}{\partial t}. \tag{22}$$

Eventually, we need an equation that describes $\mathrm{d}r/\mathrm{d}t$ (8), and therefore we rearrange (22) such that r becomes isolated from the second order differential of the derivative of space, so:

$$\sum_{n=1}^{n_p}\left(\underbrace{\frac{\partial}{\partial x}\left(K^{x}\frac{\partial p_n}{\partial x}\right)}_{u^{\mathrm{c}}_n} + \underbrace{\frac{\partial}{\partial y}\left(K^{y}\frac{\partial p_n}{\partial y}\right)}_{u^{\mathrm{r}}_n} + \underbrace{\frac{\partial}{\partial z}\left(K^{z}\frac{\partial p_n}{\partial z}\right)}_{u^{\mathrm{v}}_n} - \underbrace{C^{\mathrm{s}}p_n}_{u^{\mathrm{w}}_n}\right) r_n = w^{\mathrm{s}} - C^{\mathrm{s}}(h_{\mathrm{riv}} - h_{*}) + \sum_{n=1}^{n_p}\underbrace{S^{\mathrm{s}}p_n}_{u^{\mathrm{s}}_n}\frac{\partial r_n}{\partial t}. \tag{23}$$

A major advantage in this formulation is that the entire term bracketed in the left-hand side of the equation, can be computed in advance. It should be noticed that the elimination of h_{*} herein, is only sustained for these type of confined linear models as K^{x}, K^{y}, K^{z}, S^{s} are all independent of h_{*}. The removal of h_{*} that affects C^{s}, is corrected by adjusting the surface water levels h_{riv} by h_{*}. Whenever we apply upon (23) a finite-difference approximation for the pattern derivative of space, we can compute for each pattern p_n the variables u^{c}_n, u^{r}_n, u^{v}_n, u^{w}_n, u^{s}_n for each grid cell i, j, k in the mesh, as:

$$u^{\mathrm{c}}_{(i,j,k),n} = \Delta x^{-1}_{(j)}\left(C^{\mathrm{gc}}_{(i,j,k)}\frac{p^{n}_{(i,j,k)} - p^{n}_{(i,j+1,k)}}{\frac{1}{2}\left(\Delta x_{(j)} + \Delta x_{(j+1)}\right)} - C^{\mathrm{gc}}_{(i,j-1,k)}\frac{p^{n}_{(i,j,k)} - p^{n}_{(i,j-1,k)}}{\frac{1}{2}\left(\Delta x_{(j)} + \Delta x_{(j-1)}\right)}\right), \tag{24}$$

$$u^{\mathrm{r}}_{(i,j,k),n} = \Delta y^{-1}_{(i)}\left(C^{\mathrm{gr}}_{(i,j,k)}\frac{p^{n}_{(i,j,k)} - p^{n}_{(i+1,j,k)}}{\frac{1}{2}\left(\Delta y_{(i)} + \Delta y_{(i+1)}\right)} - C^{\mathrm{gr}}_{(i-1,j,k)}\frac{p^{n}_{(i,j,k)} - p^{n}_{(i-1,j,k)}}{\frac{1}{2}\left(\Delta y_{(i)} + \Delta y_{(i-1)}\right)}\right), \tag{25}$$

$$u^{\mathrm{v}}_{(i,j,k),n} = \Delta \dot{z}^{-1}_{(k)}\left(C^{\mathrm{gv}}_{(i,j,k)}\frac{p^{n}_{(i,j,k)} - p^{n}_{(i,j,k+1)}}{\frac{1}{2}\left(\Delta \dot{z}_{(k)} + \Delta \dot{z}_{(k+1)}\right)} - C^{\mathrm{gv}}_{(i,j,k-1)}\frac{p^{n}_{(i,j,k)} - p^{n}_{(i,j,k-1)}}{\frac{1}{2}\left(\Delta \dot{z}_{(k)} + \Delta \dot{z}_{(k-1)}\right)}\right), \tag{26}$$

$$u^{\mathrm{w}}_{(i,j,k),n} = C^{\mathrm{s}}_{(i,j,k)}O_{(i,j,k)}p^{n}_{(i,j,k)}, \tag{27}$$

$$u^{\mathrm{s}}_{(i,j,k),n} = S^{\mathrm{s}}_{(i,j,k)}\Delta z_{(k)}p^{n}_{(i,j,k)}, \tag{28}$$

with

$$C^{\mathrm{gr}}_{(i,j\pm1,k)} = \left(\Delta x_{(j)} + \Delta x_{(j\pm1)}\right) \Bigg/ \left(\frac{\Delta x_{(j)}}{K^{x}_{(i,j,k)}\Delta z_{(k)}} + \frac{\Delta x_{(j\pm1)}}{K^{x}_{(i,j\pm1,k)}\Delta z_{(k)}}\right), \tag{29}$$

$$C^{\mathrm{gc}}_{(i\pm1,j,k)} = \left(\Delta y_{(i)} + \Delta y_{(i\pm1)}\right) \Bigg/ \left(\frac{\Delta y_{(i)}}{K^{y}_{(i,j,k)}\Delta z_{(k)}} + \frac{\Delta y_{(i\pm1)}}{K^{y}_{(i\pm1,j,k)}\Delta z_{(k)}}\right), \tag{30}$$

$$C^{\mathrm{gv}}_{(i,j,k\pm1)} = \left(\Delta \dot{z}_{(k)}\Delta \dot{z}_{(k\pm1)}\right) \Bigg/ \left(\frac{\frac{1}{2}\Delta z_{(k\pm1)}}{K^{\mathrm{v}}_{(i,j,k\pm1)}} + \frac{\Delta z^{\mathrm{s}}_{(k\pm1)}}{K^{\mathrm{s}}_{(i,j,k\pm1)}} + \frac{\frac{1}{2}\Delta z_{(k)}}{K^{\mathrm{v}}_{(i,j,k)}}\right). \tag{31}$$

Within this Galerkin model the C^{gr}, C^{gc}, C^{gv} are the confined harmonic mean hydraulic conductances ($\mathrm{L^2T^{-1}}$) between nodes along the rows, columns and layers, respectively; $\Delta\dot{z}$ is the fictitious distance between nodes along the vertical direction and is equal 1.0, the true vertical distance Δz has been used already in the computation of C^{gv} (31). O is the wetted area of the streambed times the total length of the streambed in a grid cell ($\mathrm{L^3}$); and p^n is the nth pattern value out of n_p (–).

The entire set of equations can be summarized in matrix form, as:

$$\underbrace{\left(\mathbf{U}^{\mathrm{c}} + \mathbf{U}^{\mathrm{r}} + \mathbf{U}^{\mathrm{v}} - \mathbf{U}^{\mathrm{w}}\right)}_{\mathbf{U}}\mathbf{r} = \mathbf{U}^{\mathrm{s}}\frac{\mathrm{d}\mathbf{r}}{\mathrm{d}t} + \underbrace{\mathbf{w}^{\mathrm{p}} - \mathbf{C}^{\mathrm{s}}\mathbf{O}\left(\mathbf{h}^{\mathrm{p}}_{\mathrm{riv}} - \mathbf{h}_{*}\right)}_{\mathbf{b}^{\mathrm{p}}} \tag{32}$$

where $\mathbf{U}$ has dimension $[n_m \times n_p]$; $\mathbf{w}^{\mathrm{p}}$ are the source/sink terms concerning the *pattern impulses* ($\mathrm{LT^{-1}}$). The mathematical dimension (length of the vectors) of (32) is still equal to the original length n_m, though the length of the unknown vector $\mathbf{r}$ is n_p. In words: we have more equations than unknown variables. To eliminate all superfluous equations, we project (32) upon the selected set of pattern by multiplying each term with the transpose of the patterns $\mathbf{P}^{\mathrm{T}}$, so:

$$\underbrace{\mathbf{P}^{\mathrm{T}}\mathbf{U}}_{\mathbf{N}}\mathbf{r} = \underbrace{\mathbf{P}^{\mathrm{T}}\mathbf{U}^{\mathrm{s}}}_{\mathbf{M}}\frac{\mathrm{d}\mathbf{r}}{\mathrm{d}t} + \mathbf{P}^{\mathrm{T}}\mathbf{b}^{\mathrm{p}}. \tag{33}$$

This is an ODE for a reduced model for groundwater flow. We can solve (33) by applying an implicit Euler scheme of the time derivative of $\mathbf{r}$, resulting in:

$$\boxed{\left(\mathbf{N} - \frac{1}{\Delta t}\mathbf{M}\right)\mathbf{r}^{m} = -\frac{1}{\Delta t}\mathbf{M}\mathbf{r}^{m-1} + \left(\mathbf{P}^{\mathrm{T}}\mathbf{b}^{\mathrm{p}}\right)^{m}.} \tag{34}$$

This GP results in a reduced model which consists of three time-independent matrices $\mathbf{N}$ and $\mathbf{M}$—both with a small dimension $[n_p \times n_p]$—and the matrix $\mathbf{P}^{\mathrm{T}}$ with dimension $[n_p \times n_m]$. During the actual simulation $\mathbf{b}^{\mathrm{p}}$ should be multiplied with $\mathbf{P}^{\mathrm{T}}$ and after that it is easy to obtain the coefficients $\mathbf{r}^m$ because all matrices and vectors in the equation are low dimensional.

2.4.3. Initial conditions

The initial conditions $\mathbf{r}^0$ for the transient reduced models (21) and (34) can be obtained by computing:

$$\mathbf{r}^0 = \mathbf{P}^{\mathrm{T}}(\mathbf{h}^0 - \mathbf{h}_{*}), \tag{35}$$

where $\mathbf{h}^0$ is the initial hydraulic head. Eq. (35) is only meaningful if $\mathbf{h}^0 - \mathbf{h}_{*}$ can be described perfectly by the set of patterns.

2.5. Discussion

2.5.1. Time discretisation

Both, stress-periods and time-steps as defined by MODFLOW [10], can be used by the reduced models. Nevertheless, there is an important difference in their formulation that affects the implementation of these time scales during a simulation:

- *State-Space Projection SSP*: within this formulation, Δt^m is included within the computation of the matrices $\mathbf{N}$ and $\mathbf{M}$, see Section 2.4.1 for elaboration. To avoid these Δt-dependent computations, as they completely undermine the gained computational effort, we suggest a more practical solution. Hereby the concerned matrices are computed for a specific Δt that is capable to follow the evolution of the desired time-steps; this could be the smallest Δt within the simulation, for example 10 days. Whenever Δt changes during the simulation into e.g. 30 days, we solve $\mathbf{r}$ for the intermediate periods (10, 20 days) without recomputing $\mathbf{M}^{\mathrm{T}}\mathbf{b}^{\mathrm{p}}$ (21). This will hardly increase the computational time;
- *Galerkin Projection GP*: a change in Δt^m does not affect the reduced model that severe as within a SSP. There is no limitation for a variation in Δt^m as the finite-difference approximation of $\mathrm{d}\mathbf{r}/\mathrm{d}t$ has been computed after the actual projection (33). As a result, Δt can be varied unlimited at low computational costs, as it affects low-dimensional matrices only (34).

2.5.2. Numerical aspects

There is an important difference between the SSP and GP methods, that concerns the stage at which the actual projection is applied. The GP can be summarized by the following sequence of equations:

$$\mathbf{A}\mathbf{h} = \mathbf{b} \overset{\text{projecting}}{\Rightarrow} \mathbf{P}^{\mathrm{T}}\mathbf{A}\mathbf{P}\mathbf{P}^{\mathrm{T}}\mathbf{h} = \mathbf{P}^{\mathrm{T}}\mathbf{b} \Longleftrightarrow \mathbf{r} = \underbrace{\left(\mathbf{P}^{\mathrm{T}}\mathbf{A}\mathbf{P}\right)^{-1}}_{\widehat{\mathbf{N}}}\mathbf{P}^{\mathrm{T}}\mathbf{b}, \tag{36}$$

where $\mathbf{A}$ reflects the system matrix and $\mathbf{b}$ the forcing terms. It should be noticed that $\mathbf{A}$ is projected upon the patterns prior to the computation of an inverse. This is very efficient because the dimension is first significantly reduced, but it can lead to serious errors in $\widehat{\mathbf{N}}$. For this

particular error the SSP is more accurate, as shown by the following sequence of equations:

$$\mathbf{h} = \mathbf{A}^{-1}\mathbf{b} \overset{\text{projecting}}{\Rightarrow} \mathbf{P}^{\mathrm{T}}\mathbf{h} = \mathbf{P}^{\mathrm{T}}\mathbf{A}^{-1}\mathbf{P}\mathbf{P}^{\mathrm{T}}\mathbf{b} \Longleftrightarrow \mathbf{r} = \underbrace{\mathbf{P}^{\mathrm{T}}\mathbf{A}^{-1}\mathbf{P}}_{\mathbf{N}}\mathbf{P}^{\mathrm{T}}\mathbf{b}. \tag{37}$$

The advantage of this SSP is its inclusion of $\mathbf{A}^{-1}$. Therefore we assign $\mathbf{N}$ as the truth, and $\widehat{\mathbf{N}}$ as an approximation due to its a priori projection. The "extra" mathematical error caused by the difference between $\mathbf{N}$ and $\widehat{\mathbf{N}}$ is negligible whenever the following conditions are met:

(1) We should include the entire numerical space of the original model; in other words: all variance should be explained by the reduced model ($\varphi^{\mathrm{e}} = 100\%$). In practice this will be never the case, as it conflicts with the concept of a reduced model: that is to include the smallest number of patterns and still obtain reliable results.
(2) The snapshots should represent the behaviour of the model most accurately. For a simple model we can approach that condition; as for more complex models this is difficult and the resulting patterns with tiny eigenvalues are numerically ill defined. The SSP method introduces errors due to these (unreliable) patterns, as they contribute to the inverse at their full vector dimension (n_m). The GP suffers less, because the vector dimension, of the unreliable patterns, is reduced significantly (n_p), prior to the inverse computation.
(3) The round-off errors accumulate with the number of grid cells (n_m) and patterns (n_p). For the SSP this error will play a more important role as we need to solve $\mathbf{P}^{\mathrm{T}}\mathbf{A}^{-1}$ iteratively.

From the above-mentioned items we conclude that the mathematical formulations of both methods have certain advantages and disadvantages. To evaluate their performance we have applied them to a realistic case.

3. Realistic case study

In this section we describe the performance of a reduced model based upon a SSP and GP. We applied them upon a realistic, supra-regional model with a high degree of variability in aquifer properties, recharge and surface water elements.

3.1. Description of the original model

The underground of the model is a complex system of successive high and extremely low permeabilities (Figs. 2 and 3) and is modeled by 9 model layers in which several extraction wells are active. The entire model contains 61,632 nodes, of which $n_m = 32{,}949$ are active. All others are inactive (no-flow) due to an irregular boundary and/or several aquifers which thin out.

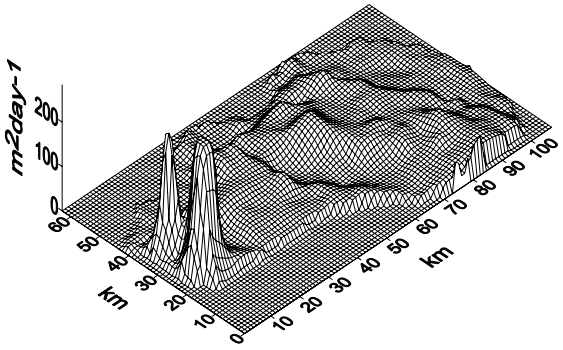

Fig. 2. Spatial structure of the horizontal conductance $K\,\Delta z$ ($\mathrm{m^2\,day^{-1}}$) for model layer 1.

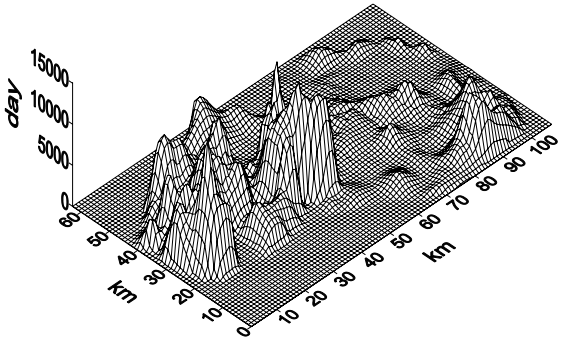

Fig. 3. Spatial structure of the vertical resistance $\frac{\Delta z^{\mathrm{s}}}{K^{\mathrm{s}}}$ (day) between model layer 1 and 2.

The groundwater model is characterized by regional areas with free-floating water tables and regions with intense surface water systems. The latter dewaters and recharges in proportion to the difference between h and h_{riv}. This is a linear relationship and is modelled with the GHB-package within MODFLOW. The RCH-package is used to simulate the precipitation and evaporation. Hence, the model is strictly linear. Finally, an open boundary condition has been modelled by constant head cells for each model layer, all around.

The main purpose of the reduced model was to evaluate whether it could simulate the long-term effects of change in precipitation/evaporation, together with the impact of variable pumping rates for all extraction wells simultaneously for the model layers $2, \ldots, 9$. So, the reduced model should be able to vary $n_{\mathrm{v}} = 9$ groups (recharge/evaporation and eight layers with wells) independently. We varied the rates within each group randomly and simulated 25 stress-periods divided into 150 time-steps, each $\Delta t = 10$ days.

3.2. Resulting patterns

To find appropriate patterns to simulate the desired scenarios, we filled a data set with an ensemble of snapshot vectors obtained by the original model. To minimize the data set, we took the linearity of the model into account. As a result of that, we were able to compute a combined effect for different groups, by combining their individual responses (*superposition*). Whenever we consider a steady-state simulation, we need to fill the data set with the steady-state responses for each group; so $n_e = n_v = 9$. For our transient simulation we need the patterns to capture the entire response behaviour over time; so $n_e = \alpha \cdot n_v$. For each group the factor α defines the number of snapshots that are neccessary to describe its response. After analyzing the behaviour of the individual responses, (Fig. 4) we collected the following snapshots: nine snapshots to describe the recharge response: $\Delta t^{m+1} = 2\Delta t^m$ with $\Delta t^1 = 10$ days; and four snapshots to describe the response caused by each well group: $\Delta t^1 = 10$, $\Delta t^2 = 10$, $\Delta t^3 = 50$, $\Delta t^4 = 250$ days. It should be noticed that the chosen time steps are not by definition the best, different combinations will improve of worsen the performance of the reduced model. The most important issue herein is that the frequency should be high initially and may be decreased as time elapses until a steady-state solution is reached [14].

Finally, the resulted data set contained $n_e = 43$ snapshot vectors in total, including a zero-vector $\mathbf{h}_0$. With the $n_e = 43$ snapshot vectors we computed the patterns as described in Section 2.3; the relative eigenvalues φ_n are given in Fig. 5. The maximal explained variance for a pattern ($\varphi_1 = 20.42\%$) declines rapidly ($\varphi_n \ll 1\%$; $n \in \{9, \ldots, 28\}$). Even though we constructed our 43 snapshots carefully, the contribution of φ_n, $n \in \{29, \ldots, 43\}$ to the total explained variance φ_n^e is negligible. It mainly depends on the usage of a reduced model, but it is wise to collect as many patterns as needed to obtain at least $\varphi^e = 99\%$. For this realistic case we needed at least $n_p = 16$ patterns, in other words, *we have reduced the original model, which operated within 32,949 dimensions, to a model which operates within 16 dimensions only*. Apparently the spatial distribution of h is complex (n_m-dimensional) but its behaviour in time is not complex at all (n_p-dimensional) [7,14,16]. The cost of it in terms of model accuracy is negligible (see Section 3.3 for elaboration).

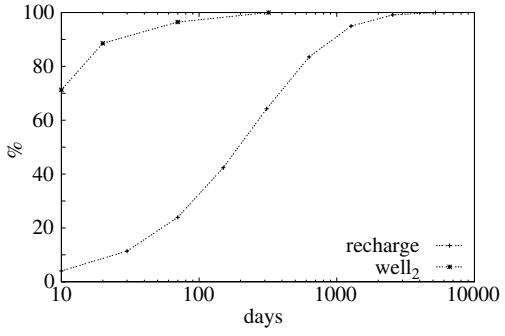

Fig. 4. Graph of the time response for different groups, towards 99% of the total steady-state response.

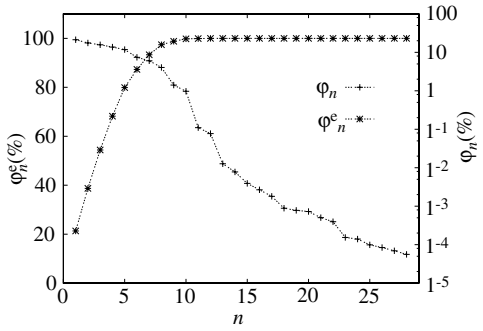

Fig. 5. Relative eigenvalues φ_n and expected variance φ_n^e versus pattern number n.

The spatial structure of a major pattern $\mathbf{p}_1$ (Fig. 6) and a minor pattern $\mathbf{p}_{19}$ (Fig. 7) is plotted. Especially the important patterns ($\varphi_n > 1\%$) are strongly related to the amplitude of the variance of the hydraulic head. Peak values within a pattern emphasizes areas within the

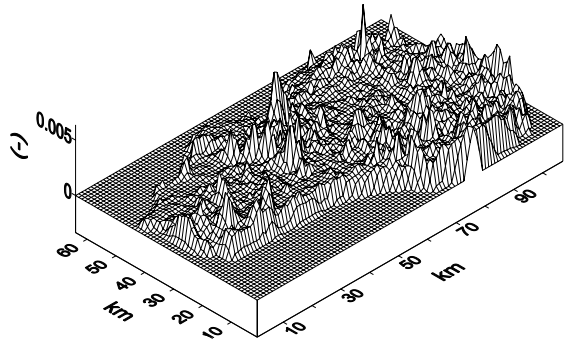

Fig. 6. Spatial structure of pattern $\mathbf{p}_1$ ($\varphi_1 = 20.424\%$) for model layer 1.

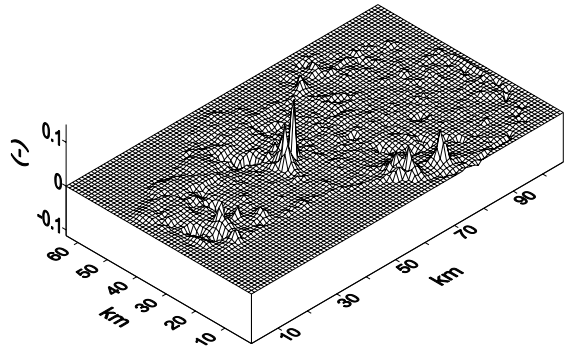

Fig. 7. Spatial structure of pattern $\mathbf{p}_{19}$ ($\varphi_{19} = 0.00091\%$) for model layer 1.

model that are strongly influenced by external sources. Within $\mathbf{p}_1$ for model layer 1 the influence of recharge can be recognized, within the minor pattern $\mathbf{p}_{19}$ for model layer 1, the influence of several specific wells can be still observed.

3.3. Accuracy

The accuracy of a reduced model is expressed as the Relative Mean Absolute Error:

$$\mathrm{RMAE} = 100 \cdot \frac{1}{n_\mathrm{t}} \sum_{m=1}^{n_\mathrm{t}} \frac{\left|\mathbf{h}^m - \hat{\mathbf{h}}^m\right|}{\left|\mathbf{h}^m - \mathbf{h}_*\right|} \ [\%], \tag{38}$$

and the Relative Root Mean-Square error [13]:

$$\mathrm{RRMS} = 100 \cdot \frac{1}{n_\mathrm{t}} \sum_{m=1}^{n_\mathrm{t}} \sqrt{\frac{\left\|\mathbf{h}^m - \hat{\mathbf{h}}^m\right\|^2}{\left\|\mathbf{h}^m - \mathbf{h}_*\right\|^2}} \ [\%]. \tag{39}$$

Both errors give a percent error conditioned on the difference between h and h_*. In this approach we accept larger errors as the difference between h and h_* increases. We have computed the RMAE and the RRMS for the SSP and GP method over $n_\mathrm{t} = 150$ time-steps (see Figs. 8 and 9).

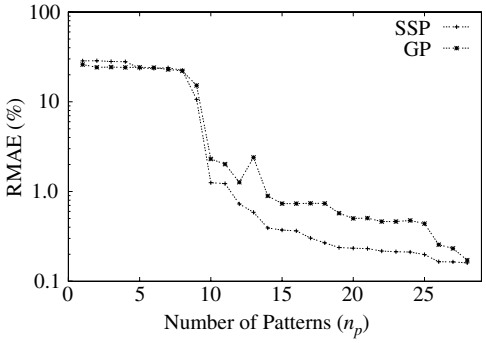

Fig. 8. Graph of n_p versus the error RMAE for the GP and SSP method over $n_\mathrm{t} = 150$ time steps.

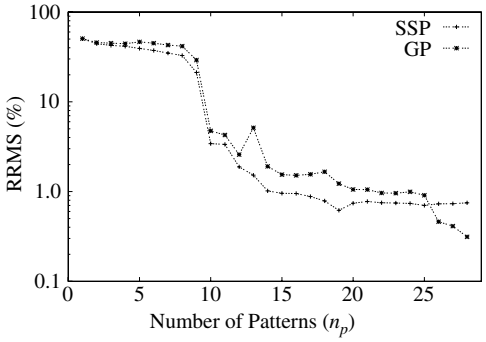

Fig. 9. Graph of n_p versus the error RRMS for the GP and SSP method over $n_\mathrm{t} = 150$ time steps.

The strong reduction in RMAE and RRMS between $n_p = 9$ and $n_p = 10$ can be explained by the fact that the reduced model simulates scenarios with 9 independent groups (Section 3.1; third paragraph) and hence beyond that point, the accuracy gathers strength. Of course, it is strongly related to the purpose of the reduced model, but an error of RMAE = 0.5% and RRMS = 1.0% should be acceptable. It should be remarked that the SSP reaches this criterion at $n_p = 16$, whereas the GP reaches this accuracy at $n_p = 24$. The latter is affected by the additional numerical error (Section 2.5.2, item 1), that can increase the inaccuracy temporary (e.g. $n_p = 13$) but declines eventually whenever n_p is enlarged. This is supported by the fact that whenever $n_p = 28$, the RMAE becomes almost similar for the SSP and GP method. For both methods the RMAE declines eventually when we include more patterns. This does not happen in the plot of RRMS for the SSP as it is more sensitive to the inclusion of unreliable patterns ($\varphi_n < 0.001\%$; $n \in \{18, \ldots, 28\}$) than the GP (Section 2.5.2 item 2–3).

To analyse both methods, we computed $\mathbf{r}$ directly from the results obtained with the original model, and marked them as the truth, so:

$$\bar{\mathbf{r}}^m = \mathbf{P}^\mathrm{T}(\mathbf{h}^m - \mathbf{h}_*). \tag{40}$$

To quantify how well each of the time-dependent coefficients r, computed with the different projection methods, resembles $\bar{r}$ we computed:

$$\epsilon(n) = 100 \cdot \sqrt{\frac{\sum_{m=1}^{n_\mathrm{t}} \left(\bar{r}_n^m - r_n^m\right)^2}{\sum_{m=1}^{n_\mathrm{t}} \left(\bar{r}_n^m\right)^2}} [\%], \tag{41}$$

for each coefficient r_n separately. Whenever we plot $\epsilon(n)$ for the SSP and GP method (Fig. 10), we see that the coefficients r_n; $n \in \{18, \ldots, 28\}$ show a large inaccuracy (50–110%). They correspond to patterns with very small eigenvalues ($\varphi_n < 0.001\%$, Fig. 5) that are numerically unreliable. This phenomenon affects the SSP more seriously than the GP. It should be noticed that patterns

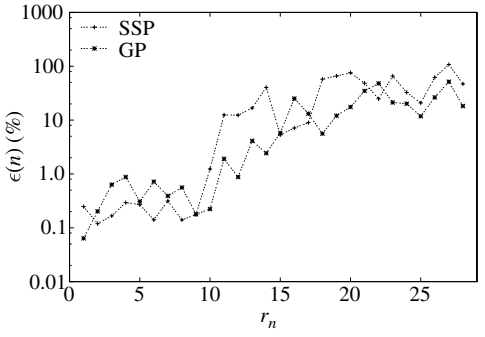

Fig. 10. Time-dependent coefficient r_n versus the error $\epsilon(n)$ over $n_\mathrm{t} = 150$ model evaluations for the GP and SSP method.

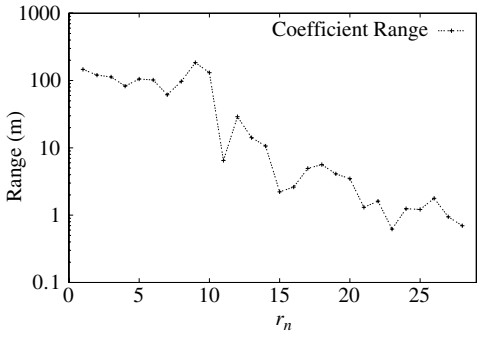

Fig. 11. Graph of the range for each time-dependent coefficient r_n over $n_t = 150$ time steps for the GP and SSP method.

with tiny φ-values contribute limited to the complete solution of $\hat{\boldsymbol{h}}$, as their r_n range (maximum r_n-value minus minimum r_n-value) is significantly (almost two orders of magnitude) smaller (see Fig. 11).

3.4. Preparation time

The key concept of a reduced model is to compute time-independent matrices in advance and to compute as little as possible during the actual simulation. The GP and SSP formulations differ, hence each requires a different computational effort to prepare their matrices **N** and **M**. We have plotted the preparation time (t^{p}) for both methods and they are both linearly related to n_p (Fig. 12). For an acceptable reduced model $t^{\mathrm{p}}_{\mathrm{SSP}} \approx 26$ s ($n_p = 16$) and $t^{\mathrm{p}}_{\mathrm{GP}} \approx 13$ s ($n_p = 24$). The SSP method consumes more time because equation (20) needs to be solved $n_p = 16$ times. For both methods, t^{p} summed with the total time taken by the computation of the $n_e = 43$ snapshots is still significantly less than one simulation of the original model (≈240 s). Therefore it is wise to create a reduced model for a limited range of scenarios, and recreate it whenever the specifications (conductances and/or positions of external sources) for the scenarios changes. In that case, fewer patterns are required for scenarios, that benefits the simulation time.

3.5. Simulation time

To quantify the efficiency (E) of the reduced models, we divided the total time taken by the PCG-solver of MODFLOW (t^{s}) to solve $\mathbf{h}^m$, by the total time taken by the reduced models ($t^{\mathrm{s}}_{\mathrm{SSP}}, t^{\mathrm{s}}_{\mathrm{GP}}$) to solve $\mathbf{r}^m$. It results in an $E_{\mathrm{SSP}} = t^{\mathrm{s}}/t^{\mathrm{s}}_{\mathrm{SSP}} \approx 625$ ($n_p = 16$) and an $E_{\mathrm{GP}} = t^{\mathrm{s}}/t^{\mathrm{s}}_{\mathrm{GP}} \approx 70$ ($n_p = 24$). The SSP method contains one matrix multiplication less and profits from the effort put in the preparation phase (Section 3.4). Although E_{SSP} and E_{SSP} decreaes whenever we add more patterns (Fig. 13), the gained time reduction remains enormous for both methods.

With a simple model we examined how E relates to n_p, n_m, the number of external sources n_q, and the complexity of the original model ξ. We took a one-layered model with constant grid cell dimensions and a constant conductance of 100 $\mathrm{m^2\,day^{-1}}$ ($\xi = 1.0$). We put a Dirichlet boundary condition on the left and right edges, and recharge within each grid cell and distributed 5 independent extraction wells throughout the model, so $n_q = n_m$. We have varied n_m and n_p and found by regression (regression coefficients $R^2 > 0.98$) the following relationship for:

$$E_{\mathrm{SSP}} = \xi \frac{n_m}{n_q} 0.40 n_m^{0.48} \frac{5}{n_p} \tag{42}$$

and

$$E_{\mathrm{GP}} = \xi \frac{n_m}{n_q} 0.12 n_m^{0.41} \frac{5}{n_p}. \tag{43}$$

The ratio n_m/n_q determines the efficiency that can be obtained by multiplying only the non-zero elements within $\mathbf{b}^{\mathrm{p}}$ ((21) and (34)). It is purely a gained time reduction through an optimized multiplication routine, that can be significant. An important conclusion from Eqs. (42) and (43) is that the efficiency increases with n_m and decreases with n_p. We have plotted a graph of E_{SSP} and E_{GP} for $\xi = 1.0$ and $n_m/n_q = 1.0$ in Figs. 14 and 15. Although E_{GP} is approximate one order of magnitude less than E_{SSP}, both methods remain still efficient when

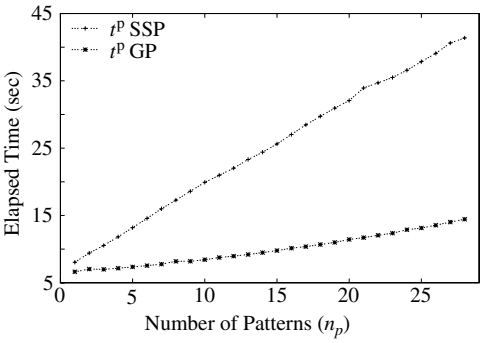

Fig. 12. Graph of n_p versus the preparation time t^{p} for the GP and SSP method.

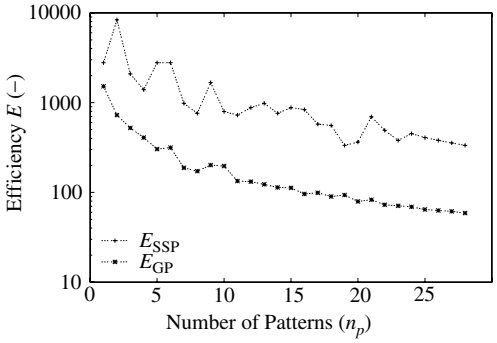

Fig. 13. Graph of n_p versus the efficiency E for the GP and SSP method.

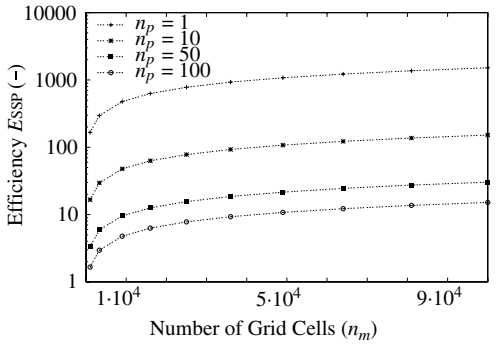

Fig. 14. Graph of n_m for a hypothetical model ($n_m/n_q = 1.0$, $\xi = 1.0$) versus the efficiency E_{SSP} for different number of patterns n_p.

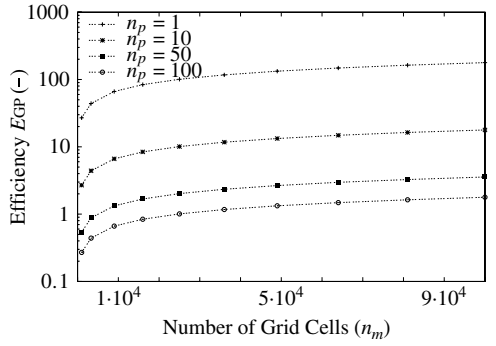

Fig. 15. Graph of n_m for a hypothetical model ($n_m/n_q = 1.0, \xi = 1.0$) versus the efficiency E_{GP} for different number of patterns n_p.

n_p increases ($n_p \approx 100$). The total efficiency is most likely higher for a practical application. Namely, for our realistic case study it appeared that $n_m/n_q = 7.1$ and $\xi \approx 5$.

3.6. Results

In Figs. 16 and 18 the mean hydraulic head

$$\bar{\mathbf{h}}_{\text{original}} = \frac{1}{n_t}\sum_{m=1}^{n_t}\mathbf{h}^m \tag{44}$$

over $n_t = 150$ time steps is plotted, as computed with the original model. In Figs. 17 and 19 we have plotted the mean hydraulic head as computed with a reduced model ($\bar{\mathbf{h}}_{\text{reduced}}$). The model is based upon a SSP with $n_p = 16$ patterns, and it is very well capable of simulating hydraulic heads within a complex distribution of permeabilities and external sources.

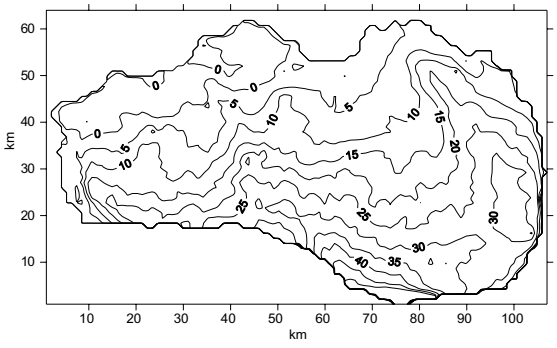

Fig. 16. $\bar{\mathbf{h}}_{\text{original}}$ for model layer 1.

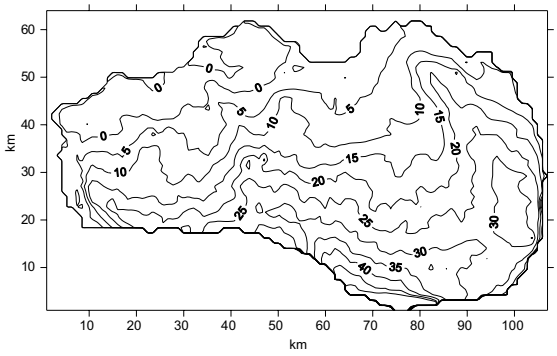

Fig. 17. $\bar{\mathbf{h}}_{\text{reduced}}$ for model layer 1.

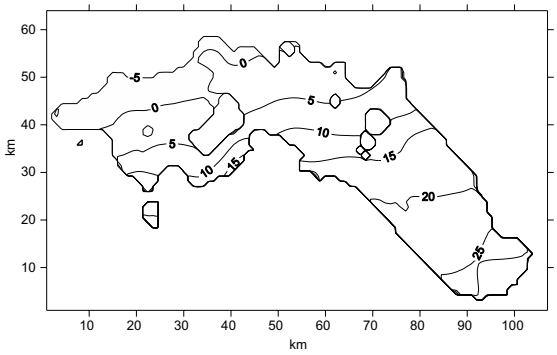

Fig. 18. $\bar{\mathbf{h}}_{\text{original}}$ for model layer 9.

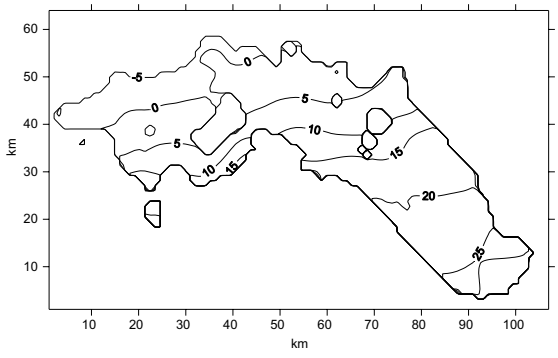

Fig. 19. $\bar{\mathbf{h}}_{\text{reduced}}$ for model layer 9.

It is interesting to see what RMAE (38) looks like as we compute it for each individual grid cell i, j, k, as:

$$\text{RMAE}_{(i,j,k)} = 100 \cdot \frac{1}{n_t}\left(\frac{\sum_{m=1}^{n_p}\left|h^m_{(i,j,k)} - \hat{h}^m_{(i,j,k)}\right|}{\Delta h_{(i,j,k)}}\right)\ [\%]. \tag{45}$$

For each grid cell i, j, k the relative error $\mathrm{RMAE}_{(i,j,k)}$ is weighted based on $\Delta h_{(i,j,k)}$, which is the maximum fluctuation for grid cell i, j, k, defined as:

$$\Delta h_{(i,j,k)} = \max\left(\left|h^m_{(i,j,k)} - h_{*,(i,j,k)}\right|\right); \quad m \in \{1,\ldots,n_t\}. \tag{46}$$

The results of these computations are given for model layer 1 in Figs. 20 and 21, and although the RMAE $\approx 0.5\%$ (Fig. 8), we see that $\mathrm{RMAE}_{(i,j,k)}$ actually varies. The enlarged errors appear especially in the regions with an intense dewatering system ($\mathrm{RMAE}_{(i,j,k)} \approx 2\%$) and near the major extraction wells ($\mathrm{RMAE}_{(i,j,k)} \approx 6\%$). The disturbance of the hydraulic head by external sources is less within model layer 9, and hence the $\mathrm{RMAE}_{(i,j,k)}$ is significant reduced.

In Fig. 22 we have plotted a time series for a specific grid cell i, j, k that has $\mathrm{RMAE}_{(i,j,k)} \approx 6\%$. Most of the time $\hat{\boldsymbol{h}}$ follows the behaviour of h accurately, but at several time steps the difference is enlarged (e.g. $t = 350$ days; $\hat{\boldsymbol{h}} - h \approx 0.15$ m). These (temporary) errors are caused by a lack of patterns, as we explain only $\varphi^e = 99\%$ with the selected set of $n_p = 16$ patterns. The absence of some or all of the rejected patterns (φ_n; $n \in \{17,\ldots,28\}$) is the cause of this specific misbehaviour—and we could include them to decrease the error. It should be mentioned that this error only occurs very locally within the model and most of the grid cells perform rather well with a $\mathrm{RMAE}_{(i,j,k)} \ll 6\%$. In Fig. 23 we have plotted a time series which possesses $\mathrm{RMAE}_{(i,j,k)} \approx 0.5\%$. Here, the reduced model simulates the behaviour of the model almost perfectly.

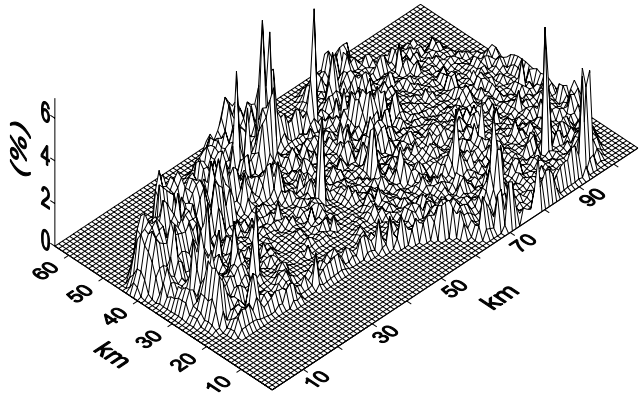

Fig. 20. $\mathrm{RMAE}_{(i,j,k)}$ for model layer 1.

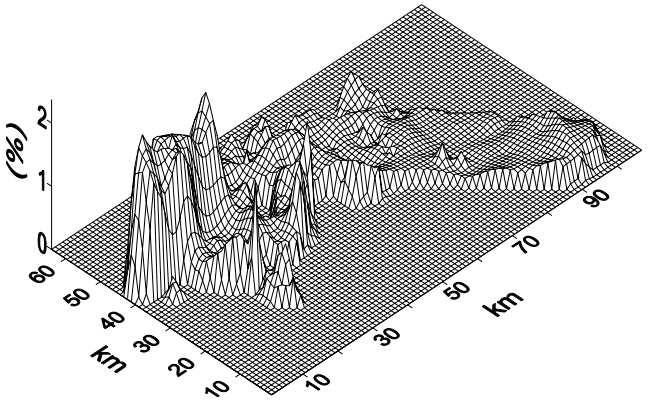

Fig. 21. $\mathrm{RMAE}_{(i,j,k)}$ for model layer 9.

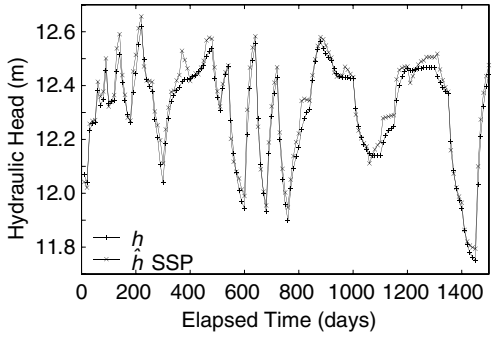

Fig. 22. Time series of h and $\hat{\boldsymbol{h}}$ (SSP) for a grid cell in the model that has $\mathrm{RMAE}_{(i,j,k)} \approx 6\%$.

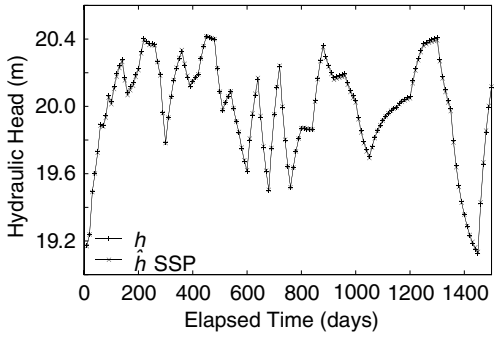

Fig. 23. Time series of h and $\hat{\boldsymbol{h}}$ (SSP) for a grid cell in the model that has $\mathrm{RMAE}_{(i,j,k)} \approx 0.5\%$.

4. Conclusions and future directions

This paper describes two methods to develop a reduced model of a linear numerical groundwater flow model. We defined a reduced model structure that consists of a set of spatial patterns with time-varying coefficients. The patterns are called Empirical Orthogonal Functions (EOFs), and they span a subspace of model results that captures most of the relevant information of the original model. The time-varying coefficients are derived by projecting the original model onto the orthogonal EOFs, starting from a partial differential equation (Galerkin Projection GP) and from a state-space formulation (State-Space Projection SSP). We have used the two different projection strategies to simulate different scenarios with a realistic case study. Both methods were able to simulate the scenarios within an

acceptable accuracy constraint (Relative Mean Absolute Error RMAE < 0.5%). To obtain this accuracy we needed more patterns for a GP (24) than for a SSP (16). This is caused by an additional error which affects only the GP, but decreases whenever we include more patterns. Due to its mathematical formulation, the SSP is numerically more sensitive to round-off errors, especially with patterns that explain a very small amount of variance ($\varphi_n \ll 0.001\%$) of the original model. Another consequence of its formulation is that the reduced model contains one matrix multiplication less than the one created by a GP. Therefore we achieved a larger time reduction with a SSP than with a GP. Specific for the realistic case study, explained in this paper, we achieved an efficiency (time reduction) of $\approx$625 and $\approx$70, respectively. For both methods, the efficiency increases with the number of grid cells and the complexity of the model.

In future research we intend to focus on the possibility to apply the discussed reduced model to non-linear three-dimensional groundwater flow models. Experiences from other sciences showed that the reduced model is also valuable in parameter estimation [3,14] and in the computation of the Reduced Order Kalman Filters [6]. These topics have our interest also.

References

[1] Adomaitis RA. RTCVD model reduction: a collocation on empirical eigenfunctions approach. Technical Report T.R. 95-64, Inst Systems Research, University of Maryland in College Park, MD, 1995.

[2] Cazemier W, Verstappen RWCP, Veldman AEP. Proper orthogonal decomposition and low-dimensional models for driven cavity flows. Phys Fluids 1998;10:1685–99.

[3] Dely F, Buoro A, Marsily de G. Empirical orthogonal functions analysis applied to the inverse problem in hydrogeology: evaluation of uncertainty and simulation of new solutions. Math Geol 2001;33(8):927–49.

[4] Delville J, Lamballais E, Bonnet JP. POD, LODS and LSE: their links to control and simulation of mixing layers. ERCOFTAC Bull 2000;46:29–38.

[5] Golub G, Loan van A. Matrix computations. 2nd ed. John Hopkins University Press; 1989.

[6] Heemink AW, Verlaan M, Segers AJ. Variance reduced ensemble Kalman filtering. Mon Weather Rev 2001;129(7):1718–28.

[7] Hoffmann Jørgensen B, Sørensen JN. Proper orthogonal decomposition and low-dimensional modelling. ERCOFTAC Bull 2000;46:44–51.

[8] Hooimeijer MA. Reduction of complex computational models. Delft: Sieca Repro; 2001.

[9] Krysl P, Lall S, Marsden JE. Dimensional model reduction in non-linear finite element dynamics of solids and structures. Int J Numer Meth Engng, in press.

[10] McDonald MG, Harbaugh AW. A modular three-dimensional finite-difference groundwater flow model. US Geological Survey, Open-File Report 83-875, Book 6, Chapter A1, 1988.

[11] Newman AJ. Model reduction via the Karhunen–Loève expansion—part I: An exposition. Technical Report T.R. 96-32. Inst Systems Research, University of Maryland in College Park, MD, 1996.

[12] Newman AJ. Model reduction via the Karhunen–Loève expansion—part II: Some elementary examples. Technical Report T.R. 96-33. Inst Systems Research, University of Maryland in College Park, MD, 1996.

[13] Overschee Van P, Moor De B. Subspace identification for linear systems. Theory, implementation, applications. Kluwer Academic Publishers; 1996.

[14] Park HM, Cho CH. Low dimensional modeling of flow reactors. Int J Heat Mass Transfer 1996;39(16):3311–23.

[15] Reyment RA, Jöreskog KG. Applied factor analysis in the natural sciences. Cambridge University Press; 1993.

[16] Sirovich L. Turbulence and the dynamics of coherent structures—Part I: Coherent structures. Quart Appl Math 1987;45(3):561–71.

[17] von Storch H. Statistical aspects of estimated principal vectors (EOFs) based on small sample sizes. J Climate Appl Meteorol 1985;24:716–24.

[18] Vermeulen PTM, Heemink AW, Stroet te CBM. Model Reduction In Groundwater Hydrology. In: Final Proc Int Conf on Modelling and Simulation, Canberra, Australia, vol. 1. 2001, p. 407–12.

[19] Vermeulen PTM, Heemink AW, Stroet te CBM. Reduction of large-scale numerical groundwater flow models. In: Final Proc XIV Int Conf on Computational Methods in Water Resources, Delft, the Netherlands, vol. 1. 2002, p. 397–404.

[20] Vermeulen PTM, Heemink AW, Stroet te CBM. Low-dimensional modeling of numerical groundwater flow. J Hydrol Process, in press.